Evaluation of Welding Imperfections with X-ray Computed Laminography for NDT Inspection of Carbon Steel Plates

Emad E. Ghandourah[1,4] · Shahfuan Hanif A. Hamidi[2] · Khairul Anuar Mohd Salleh[3] · Mahamad Noor Wahab[2] · Essam Mohammed Banoqitah[1,4] · Abdulsalam Mohammed Alhawsawi[1,4] · Essam B. Moustafa[5]

Abstract

X-ray computed laminography is a depth-resolving non-destructive testing technique well suited for the non-destructive examination of large and flat structures where traditional computed tomography is impractical. This technique provides 3D radiographic imaging and characterization with depth information of welding imperfections in welded components, ensuring component quality meets the standard criteria and safety purposes. Furthermore, determining the welding imperfection's location in fabrication, in-service and maintenance is crucial for welding repair, resulting in the areas where the repair work needs to be started. This work highlights the characterization of welding imperfections by experimental digital radiography with digital detector array (RT-D with DDA) and coplanar translational laminography (CTL) techniques applied to welded carbon steel plates. A test specimen was tested, specially prepared with artificial planar and volumetric flaws like lack of fusion, clustered porosities and slag inclusions with varying dimensions and the approaches were analyzed. Additionally, a test phantom was fabricated with known geometry features that access the CTL system's optimal detection accuracy to demonstrate a broad functionality and acceptance of the CTL system for depth information in the plate-like structures. The coplanar translational laminography technique provides advantages for characterizing welding imperfections and testing phantom features with high contrast and acceptable image quality. The result is confirmed by the phased array ultrasonic testing and RT-D with DDA. The exposure conditions, image sensitivity, and quality are analyzed according to ISO 17636-2 to ensure compliance with industry standards in digital radiography.

1 Introduction

Radiographic testing (RT) is a non-destructive testing (NDT) method widely used to evaluate and investigate welded component's integrity to discover discontinuities that could impair the component's strength, durability and service life.

✉ Khairul Anuar Mohd Salleh
khairul_anuar@nm.gov.my

Emad E. Ghandourah
eghandourah@kau.edu.sa

Shahfuan Hanif A. Hamidi
shahfuanh@unikl.edu.my

Mahamad Noor Wahab
mahamadnoor@unikl.edu.my

Essam Mohammed Banoqitah
ebanoqitah@kau.edu.sa

Abdulsalam Mohammed Alhawsawi
ofallatah@kau.edu.sa; am.alhawsawi@yahoo.com

Essam B. Moustafa
abmostafa@kau.edu.sa

1   Department of Nuclear Engineering, Faculty of Engineering, King Abdulaziz University, Jeddah, Saudi Arabia

2   Fabrication and Joining Section, Universiti Kuala Lumpur-Malaysia France Institute (UniKL-MFI), 43650 Bandar Baru Bangi, Malaysia

3   Radiographic Testing Digital (RT-D) Laboratory, Leading Edge NDT Technology (LENDT) Group, Industrial Technology Division, Malaysian Nuclear Agency, Bangi, 43000 Kajang, Malaysia

4   Center for Training and Radiation Prevention, King Abdulaziz University, Jeddah, Saudi Arabia

5   Mechanical Engineering Department, Faculty of Engineering, King Abdulaziz University, Jeddah, Saudi Arabia

RT employs an X-ray or gamma-ray source to penetrate the material and permanently record the results on a viewing medium like a radiographic film or a digital electronic detector [1].

The film has been traditionally used with RT but slowly replaced with digital detectors to image radiographs. Digital imaging technology was first employed in medical applications and is now used extensively in NDT. Chemicals were no longer used for film processing, which resulted in a significant reduction in inspection time. Furthermore, digital technology and image processing techniques benefit service providers significantly because they are faster, more precise, and cost-effective [2]. As a result, Digital Radiography (RT-D) has developed into a versatile tool and has emerged as one of the most potential solutions and techniques for NDT.

NDT has significantly benefited from the development of digital radiography (RT-D), particularly in weld inspection. Much research has been conducted to determine the effectiveness of the RT-D system in enhancing sensitivity in detecting welding imperfections and reducing inspection cycle time. Moreira et al. used a digital detector array (DDA) to perform RT-D on an offshore pipeline of carbon steel API5L with fabricated flaws [3]. Bavendiek et al. studied the time-saving and image quality factors in aerospace applications using Inconel welded tubing and titanium weld [4]. Real-time radiography has also been done with RT-D with DDA. Boateng et al. developed and investigated the real-time technique for crack growth observation in 3 mm welded aluminum plates [5]. They also proposed using laminography to obtain depth information on welding imperfections, which will open up new possibilities for producing three-dimensional radiographic images.

Over the last three decades, research has produced crucial information on three-dimensional (3D) radiographic images for depth information of the object. Computed Tomography (CT) was initially introduced to obtain such information for healthcare medical testing. Due to its effectiveness, this technology was implemented to assess internal 3D structures of various NDT applications such as composite, manufacturing, aerospace and weld structure integrity. However, CT requires that an object be accessible from all directions. For irradiating and examining a large and flat object, i.e., a pressure vessel plate, the unrestricted rotation from all directions of the object or source-detector manipulator system is not possible. Hence, a laminographic technique has been developed to resolve this situation.

Laminography was used initially for healthcare medical testing in 1916 [6]. Later, the laminography technique was introduced to RT-D with DDA for visualizing and depth measurement in a three-dimensional (3D) image volume, gradually replacing conventional stereo radiographic techniques in various applications [7–10]. This introduction is
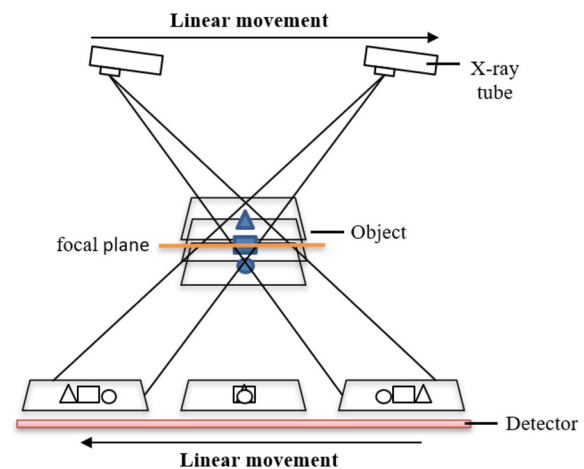

Fig. 1 Principle of laminography (adapted from [11])

prominently due to the advancement of software and hardware, such as the digital detector system applied in the NDT industry, known as Computed Laminography. In weld inspection, computed laminography can be used to determine the location of welding imperfections with depth information. This information is helpful for welding repair, resulting from which surface the repair work should be started. It is advantageous to reduce the cost and time of welding repairs. Figure 1 depicts the fundamental mechanism and principle of laminography, which employs the relative motion of the X-ray source and detector. Due to the X-ray source and detector's synchronous movements, the focus plane's internal structure will be projected onto the detector at the same position [11, 12].

Several scan geometries for the laminography system have been studied [13–16]. These include planar, circular, swing, rotary and raster. Most geometries allow the object to be imaged at high contrast and resolution based on the capabilities and calibration technique of the X-ray tube and detector. Moreover, the scan geometries with the geometrical calibration on the position of the X-ray source, object, and detector [14, 17, 18] become a necessary procedure for accurate and reliable 3D image data.

The study of each geometry requires the relative motion of the X-ray source, objects and detector. In a planar set-up (Fig. 1), the X-ray source and detector move in opposite directions. Alternatively, the X-ray source is translated along straight lines parallel to the fixed detector and the projected images are shifted during the reconstruction digitally [19, 20], as shown in Fig. 4.

This technique is established as coplanar translational laminography (CTL) [5, 21, 22] and will be used in this study since it is well suited to scan for relatively large and flat welded components. Furthermore, this geometry has several advantages for in-house and mobile testing applications [23]. This paper highlights the characterization of the
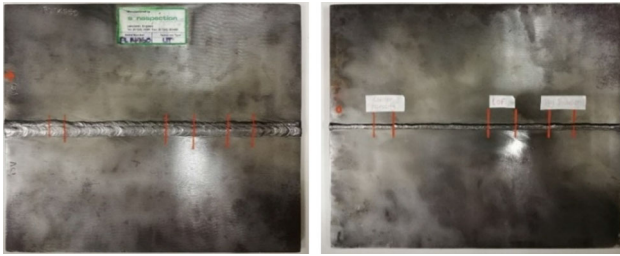
Fig. 2 Example of the test sample from the top side (left) and bottom side (right) views [12]

welding imperfections by the coplanar translational laminography (CTL) technique for flat welded carbon steel plates. It discusses the experimental approach to assessing the 2D digital radiographs image and 3D reconstructed image sample. The results show that the 2D acquired image fulfills the requirement of ISO 17636-2 (testing class A). The analysis of the 3D reconstructed image demonstrates a good agreement on depth information of the imperfections compared to the other NDT technique.

2 Research Approach

2.1 Materials

The planar and volumetric welding imperfections (clustered porosity, lack of fusion, slag inclusion) were chosen to design, model, and fabricate the welded carbon steel plate for modeling and experimental experiments. Apart from being required by code and standards, selecting these imperfections is critical since they typically emerge during fabrication and maintenance. Figure 2 shows an example of test samples. The welded plate is 300 mm × 250 mm in dimension and the base metal thickness is 8.0 mm. Weld and root reinforcements are approximately 1.5 mm and 1.0 mm, resulting in a penetrated thickness of 10.5 mm. The manufacturer (Sonaspection, UK) produced the artificial imperfections samples and issued a certificate. Table 1 tabulates the weld imperfections specification. The imperfections were measured by ultrasonic testing (UT) method. A visual assessment of the welded region was performed to confirm that it does not include open-to-surface flaws.

Additionally, a test phantom with 50 mm × 15 mm × 9.5 mm in dimension was designed and fabricated to assess the accuracy of the CTL system, especially on the consistent linear movement of the source at a constant distance to the detector. The test phantom has seven small diameter carbon steel wires (1 mm diameter) inserted into a highly precise, clear acrylic material. The lengths of wires in the range of 1.0 mm to 7.0 mm are selected to obtain the wire's depth

information, where the result has been compared to the RT-D with DDA. The schematic feature of the test phantom is shown in Fig. 3.

2.2 Data Acquisition and Evaluation

The measurements were performed on a welded carbon steel plate and test phantom at RT-D Laboratory, leading edge NDT technology (LENDT) Group at Malaysian Nuclear Agency. The samples were exposed to an X-ray radiation source with a maximum of 225 kV with a 3 mm focal spot size, while the detector is a digital detector array (DDA) XRD 1611AP with amorphous silicon plates (a-Si) and a scintillator Gd_2O_2S: Tb (GOS) sensor. The DDA has a 100 μm pixel pitch and the detector's basic spatial resolution ($SR_b^{detector}$) is 120 μm at 20% modulation, measured in accordance with ISO 17636-2:2013. The DDA analog-to-digital converter (ADC) is 16-bit and the total pixel numbers are 4096 × 4096 [24]. Appropriate precautions and calibrations of the detector are required for the best image quality with contrast sensitivity.

For image acquisition, display and analysis, ISee! Professional and public ImageJ software was used to interpret, inspect, and measure the 2D and 3D image data. Then, a set of 3D volume data of the studied sample is reconstructed by a fast shift-average algorithm (TomoPlan). TomoPlan is a 3D reconstruction software tool developed at BAM Berlin for the laminography technique [25]. The 3D volume parameters of the reconstructed image were defined and scaled by 0.1 mm × 0.1 mm × 0.1 mm based on the DDA pixel size.

Before image reconstruction into a 3D volume, the 2D image from RT-D with DDA was assessed for contrast, sensitivity, and image sharpness (basic spatial resolution, SR_b) according to ISO 17636-2 [26]. The assessment was done using two image quality indicators (IQI): (a) EN 462-1/ISO 19232-1 single wire IQI and (b) EN 462–5/ISO 19232-5 duplex wire IQI. Single-wire IQI contains a series of straight wires (with different diameters) made of material similar to the object, while duplex-wire IQI consists of 13 wire pairs made of tungsten.

For CTL, a manipulator was specially designed to carry and move the X-ray tube. The maximum distance in scan angle ranges up to 30° to the detector center, depending on the X-ray tube port opening. A driving motor was programmed so the DDA was able to acquire multiple images with a minimum speed of less than 1.0 mm/sec. The movement can be configured to acquire up to 1000 projected images by the DDA during a linear equidistant step of the X-ray source. Each projection represents the 3D object volume penetrated at a different angle. The details of the development of this system have been discussed by [27]. Tables 2 and 3 tabulate the exposure parameter of RT-D with DDA and CTL for welded

Table 1 The details of weld imperfections in the weld plate

Manufacturer	Dimension (mm)	Imperfections type	Length (mm)	Distance from 0 (mm)	Depth (mm)
Sonaspection	300 × 250 × 8.0 (thick)	Clustered porosity	15.0	46.0	5.0
		Lack of fusion	28.0	163.0	4.0
		Slag inclusion	25.0	225.0	5.0

Fig. 3 The test phantom (acrylic) feature inserted 1.0 mm carbon steel wire in the CAD model (shaded view-*left*, hidden line visible view-*right*)
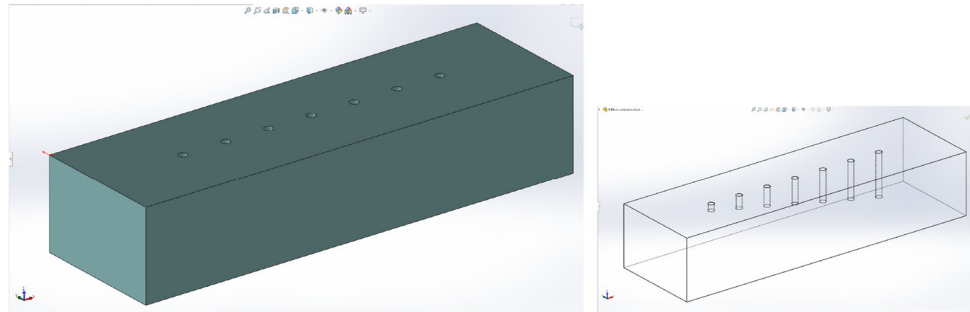
Table 2 Exposure parameters for the welded plate

Technique	X-ray voltage peak (kV$_p$)	X-ray current (mA)	Exposure/frame time (sec)	SDD (mm)	ODD (mm)	No. of frames	No. of projection	Scan angle
RT-D with DDA	160 kV	5.0	2.0	650.0	10.5	1	–	0°
CTL	160 kV	5.0	2.0	650.0	10.5	1	750	30°

plate and test phantom, respectively. Figure 4 illustrates the test arrangement of the CTL system.

For comparison of the depth information of the imperfections revealed by CTL, the test sample was inspected using the Omniscan MX2 Phased Array Ultrasonic Testing System with a 5L64-A12 probe attached to an SA12-N55S wedge. Calibration of the equipment was performed on a V1 block. The glycerin was utilized as a couplant. An encoder was attached to the probe to keep track of the probe's travel distance. The inspection report was subsequently analyzed, quantified, and reported based on presented data in A-scan, C-scan, D-scan and S-scan formats.

3 Result and Discussion

3.1 2D Image Quality Assessment
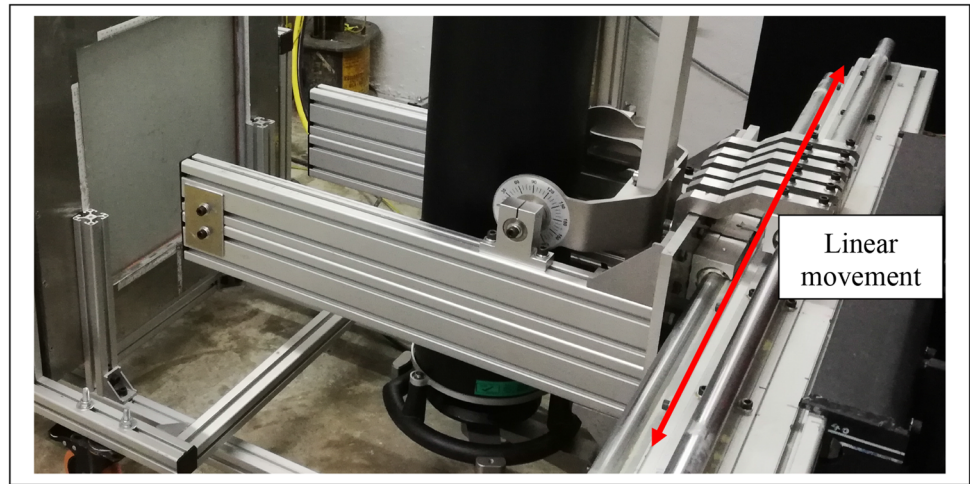
3.1.1 Welded Plate

RT-D with DDA was used to obtain the 2D digital radiographic images, as shown in Fig. 5. The image has been enhanced using a high pass filter to improve the visibility and interpretation of imperfections. As a result, the images demonstrated three welding imperfections; clustered porosity, lack of fusion (LOF) and slag inclusion. Each imperfection was measured, and the comparison was made to the standard manufacture catalog and CTL.

Prior to the imperfections evaluation, the digital radiographs image were analyzed to assess the contrast, sensitivity
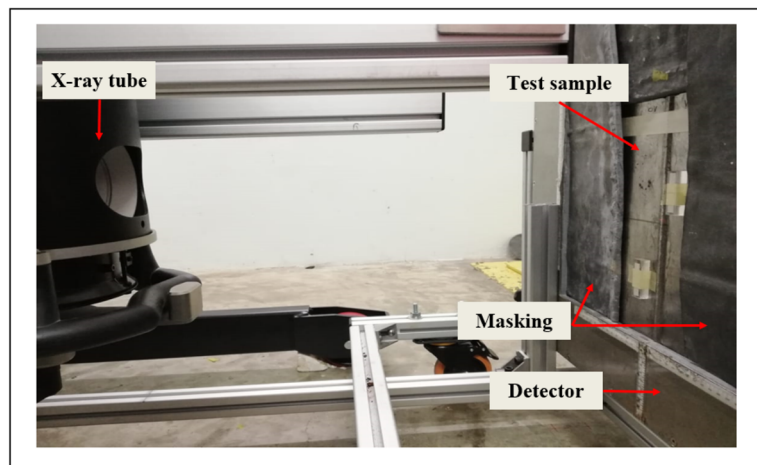
Table 3 Parameters for RT-D for test phantom

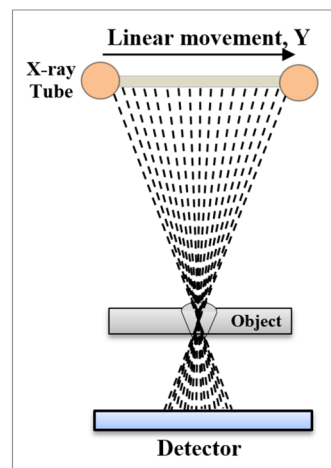| Technique	X-ray voltage peak (kV$_p$)	X-ray current (mA)	Exposure/frame time (sec)	SDD (mm)	ODD (mm)	No. of frames	No. of projection
RT-D with DDA	120 kV	2.5	10.0	1000.0	7.5	10	–
CTL	90 kV	2.0	2.0	650.0	5.0	1	700

Fig. 4 Full test arrangement of the CTL system (**a**), the position of test component (**b**) and **c** geometric configuration of coplanar translational laminography
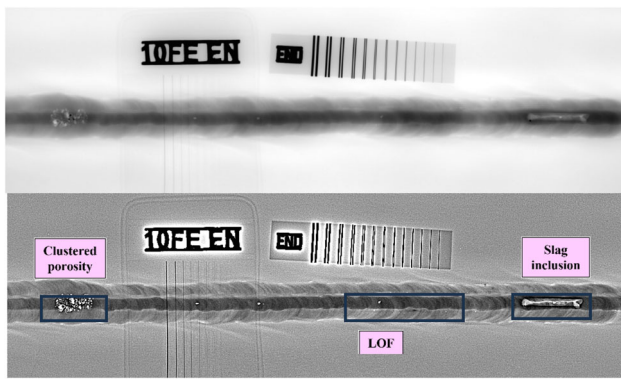

(a)

(b)

(c)

Fig. 5 Raw image (top) and filtered (bottom)

Table 4 Comparison of image quality parameters

	Single wire	Duplex wire	SR_b^{Image} mm	SNR_N at weld centre
ISO 17636-2 (Class A)	W12	D8	0.16	> 70
RT-D with DDA (raw image)	W15	D10	0.10	143

and image sharpness. The assessment was done using single and duplex IQI wires, respectively. The placement of each IQI is directly on the object's surface. Figure 6 illustrates the visibility of single wire and measurement of duplex wire IQI as a standard procedure for contrast sensitivity and image unsharpness (SR_b) [26]. The normalized signal-to-noise ratio (SNR_N) was then determined at a region of interest (ROI) of 20×55 pixel size to indicate the image quality of the radiograph's image. The result of image quality is shown in Table 4.

According to Table 4, the result demonstrated that the image quality of 2D images is well above the minimum requirement of the referred standard (testing class A). Further evaluation of images was determined by comparison to the CTL image.

3.1.2 Test Phantom

RT-D with DDA was performed at the front side of the phantom with the wires parallel to the detector to evaluate each wire's length in 2D digital radiographic images. This result is compared to the depth information obtained from the 3D reconstruction image using CTL and the wires oriented parallel to the X-ray beam. For the image quality, the assessment
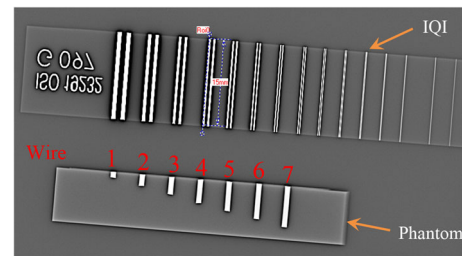

Fig. 7 The 2D image of the test phantom where scale calibration and image quality assessment by the duplex wire IQI (high pass filtered for easier visual display)

and measurement of carbon steel wire were done by the IQI duplex wire. Figure 7 illustrates the 2D image of the test phantom.

3.2 Evaluation of CTL Images

Figure 8 depicts the reconstructed welding imperfection's top (XY) and cross-sections (YZ) view for the carbon steel plate. The XY image (left) is the slice image through the reconstructed 3D dataset by the shift-average algorithm, and the analyzed region of a slice is squared with a red square.
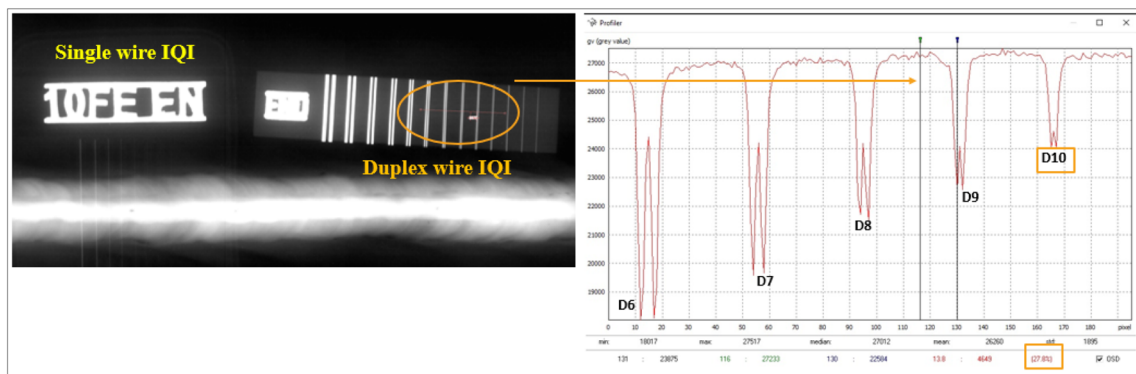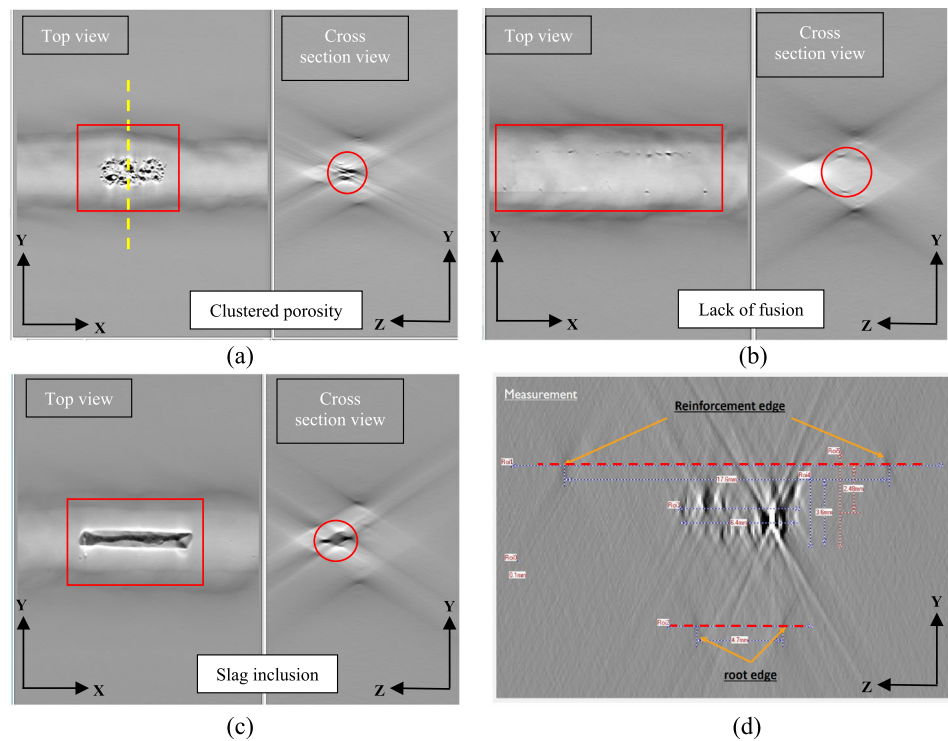

Fig. 6 The visibility of single wire and the measurement of duplex wire IQI based on ISO 19232-5

Fig. 8 The top view and cross-section view of welding imperfections. **a** clustered porosity, **b** lack of fusion, **c** slag inclusion and **d** the example measurement of the imperfection (clustered porosity)

The analyzed region was taken at slice 165 throughout the 3D volume, as shown in Fig. 12, for the entire weld imperfections. The orthogonal view of the YZ image (right) was cut through the analyzed region. The cut area is highlighted by a yellow line. The selection of the cut area is based on the dominant or massive size of the imperfection. The analysis and measurements were carried out on YZ images for all imperfections to characterize the imperfections for depth information.

The result of the depth information is tabulated in Table 6. The depth will be different along the imperfection path due to the irregular shape of the imperfection itself. Since the parameters of 3D volume have been defined during the reconstruction process, the calibration of pixel size to unit length in mm is not required. The software has directly determined the changes in contrast by plotting a single line profile on an edge-to-edge location. The profile (Fig. 9) represents the region of interest's attenuation or grey value level at a certain position. The line profile is highlighted along the horizontal line (red dashed), shown in Fig. 8d. The weld profile's reinforcement cap and root edge were first determined to indicate the imperfection's exact location within the plate as a reference for the measurement. As shown in Fig. 8d, the location of clustered porosity is near the top surface. This information is required for welding repair, resulting in the areas where the repair work needs to be started.

The same steps were applied to the 3D reconstruction data of the test phantom. Figures 10 and 11 illustrate the reconstructed image of the steel wires in the XY (top view) and
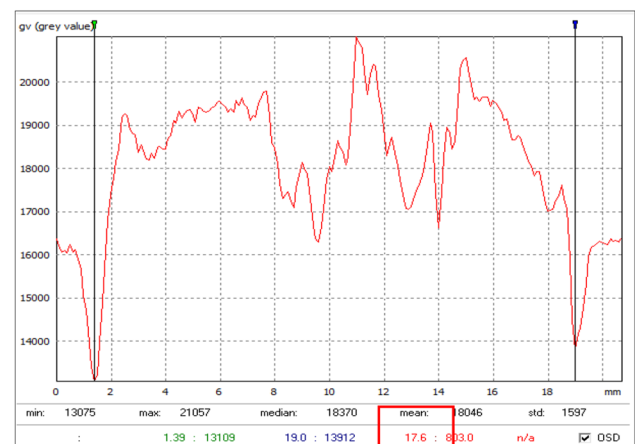

Fig. 9 The line profile across the reinforcement cap in the YZ image (cross-section view). The profile shows that the reinforcement width is 17.6 mm (red square) (Color figure online)
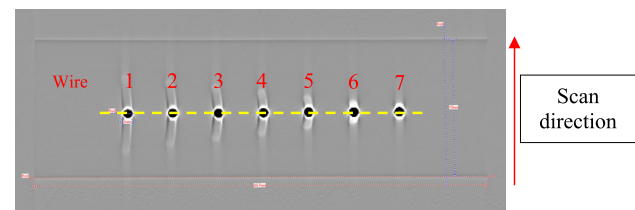

Fig. 10 The 3D reconstruction image of the test phantom at slice 172 through 3D volume in the XY plane

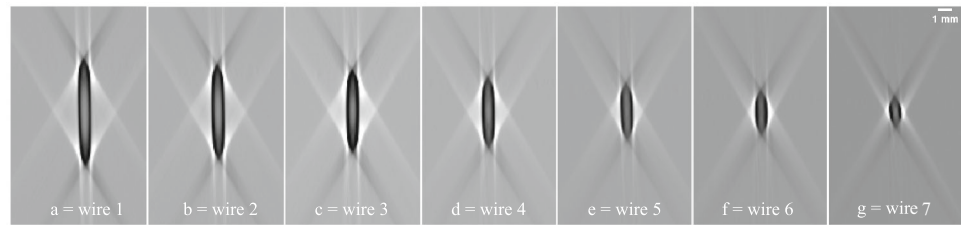**Fig. 11** The wire's cross-section view (YZ plane) at different lengths (**a–g**)

Table 5 Comparison depth of steel wire of test phantom

No	Depth (mm)		
	RT-D with DDA	CTL	Error (%)
Wire 1	7.12	7.10	0.3
Wire 2	6.10	6.16	1.0
Wire 3	4.70	4.87	3.6
Wire 4	4.06	4.10	1.0
Wire 5	3.11	3.00	3.5
Wire 6	2.10	2.09	0.5
Wire 7	1.00	1.09	9.0

YZ (cross-section view) planes. The analyzed region in the cross-section view was taken at slice 172 throughout the 3D volume. Slice 172 was taken based on the highest visibility and interpretation of all reconstructed image wires from the XY plane. The yellow line highlights the cut area through all the wires. All the measurements were carried out, and the results were compared to the 2D images. Table 5 tabulates the comparison results of the test phantom.

From Table 5, the result shows no significant difference in the wire length. The maximum percentage difference is up to 9.0%, which is acceptable for industrial practices. The differences could be due to the exposure condition, detector properties and geometrical features of the wire itself. The exposure condition and detector properties tend to influence the total image unsharpness, noise and radiation source intensity of the work object, which affects the measurement's sensitivity.

There is a drawback in measuring imperfections and wire sizes due to artifacts in the reconstructed image. To determine the exact measurement location, the sharp edge is required and will be a reference point. As for the phantom test, the measurement is started by first determining the edge-to-edge distance of the phantom with scale calibration, while the weld profile's reinforcement cap and root edge were selected to characterize the imperfections. Figures 8 and 11 depict the same artifacts developed from the reconstruction methods for the welded plate and test phantom.

Several factors were identified that contributed to this situation. One of the factors is the specifications of the X-ray tube used in this study. To avoid blurred images, the focal spot should be as small as possible to prevent massive unsharpness in the image. Even though the total image unsharpness was calculated and below the maximum required in the standard for NDT inspection, the actual depth information might become smaller from the measured data with the small focal spot size.

Another issue is the opening angle of the cone-beam for scanning trajectories. Planar geometry on flat and large components requires a large opening beam of up to $\pm\,45°$ to reduce cone beam artefacts during CTL reconstruction, which are caused by missing data and typically enlarge the depth extension.

These measurements might not deliver values of high accuracy. Still, the results were acceptable compared to the other NDT technique (RT-D with DDA), but with different orientations for depth information on imperfections.

3.3 Comparison of RT-D with DDA, CTL and PAUT

Figure 12 compares the 2D radiographic image (top image) of RT-D with DDA and the 3D reconstructed image at the slice-165 CTL of the test sample. It demonstrates that the reconstructed image provides advantages in the high contrast and image quality for visibility and measurement of imperfections.

It was clearly shown that the lack of fusion as a planar indication in the reconstructed image could be detected. These imperfections can be characterized and analyzed by measuring the cross-section image at the selected location. Hence, the disadvantage of RT in detecting and characterizing can be solved by performing a coplanar translational laminography (CTL) technique for large and flat welded components. Furthermore, there is no issue characterizing volumetric imperfections, clustered porosity, and slag inclusions. These imperfections have similar width, depth, and variable length, which RT quickly detects. Figure 13 illustrates the display of the PAUT's result and all the measurements, as shown in Table 6.

From Table 6, the results show a significant difference in the depth and height of the lack of fusion and the height of slag inclusion. The differences can be calculated up to more than 40% from the PAUT results. These issues might be due to the measurement of CTL at one location only compared to

Fig. 12 Comparison of the test sample by 2D radiographic image (top) and 3D laminographic reconstructed image (bottom) at slice-165, both high pass filtered
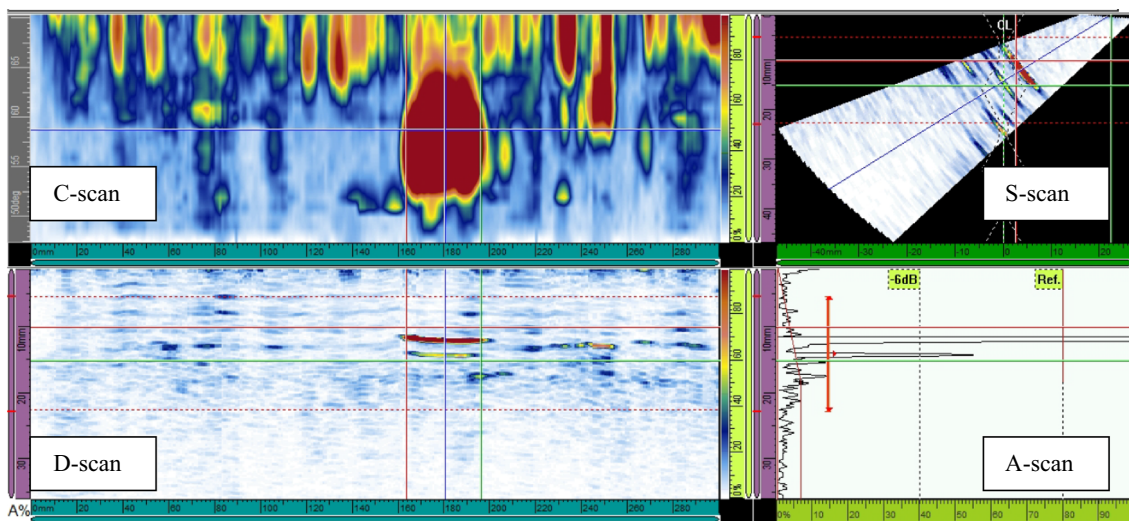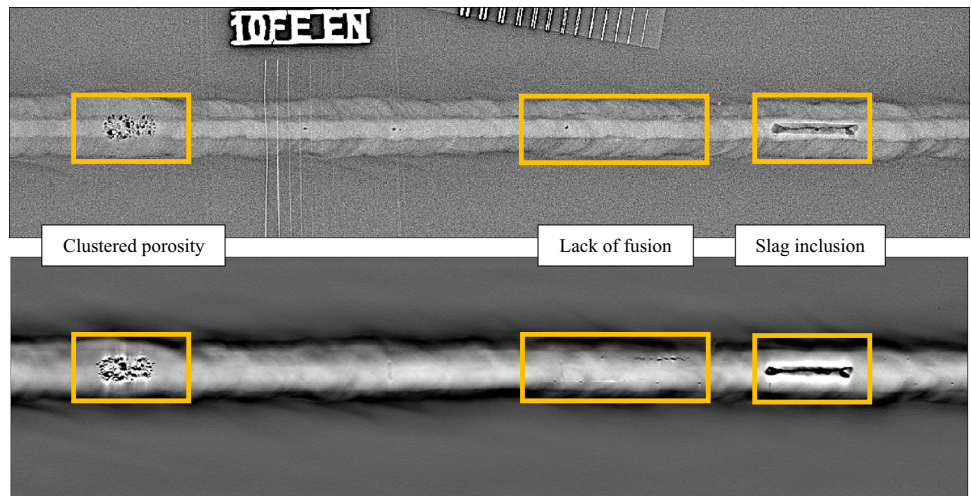

Fig. 13 Display of the PAUT's results

Table 6 Comparison of results

Type	PAUT					RT-D with DDA & CTL				
	Position (S)	Length (L)	Depth[a] (D)	Height (H)	(D) + (H)	Position (S)	Length (L)	Depth[a] (D)	Height (H)	(D) + (H)
Clustered porosity	48.0	13.0	3.4	3.3	6.7	47.0	14.0	2.5	3.6	6.1
Lack of fusion	163.0	33.0	4.0	5.2	9.2	167.0	29.7	2.8	1.7	4.5
Slag inclusion	230.0	26.0	4.1	2.6	6.7	223.0	22.9	4.4	4.8	9.2

All dimensions in-unit mm

[a]Depth measurement started from the base metal top surface to the center axis of the imperfections

the measurement of PAUT on the dominant size of the imperfection. The depth information will be different along the imperfection length due to the irregular shape of the imperfection itself. The large X-ray focal spot size used here has also significantly introduced unsharpness, reducing the lack of fusion and slag inclusion definition. However, there are no significant differences in clustered porosity depth values. It indicates that the sizing result of these imperfections by CTL was in good correspondence with the PAUT.

4 Conclusion

The analysis of the carbon steel plate with several artificial welding imperfections and a test phantom was performed using RT-D with DDA and CTL. It indicates that the approach applied is reliable for NDT inspection. The 2D radiographic image was acquired and analyzed for the welded plate according to the standard requirements. The imperfections could be detected with high contrast sensitivity and image quality using RT-D with DDA. However, the quantitative measurement of RT-D is limited by the missing depth of information. Here, the laminography technique was applied to reconstruct the missing depth information for a complete evaluation and characterization of the imperfections. The depth information, especially for large and flat welded components, is crucial for failure analysis in structural integrity. Other techniques were used, like CT, for the same purposes, but CT of large and flat structures is impractical due to the restricted scanning angle below 360° for a full data set without artefacts. Therefore, it can be concluded that CTL is the best technique for 3D measurement with restricted access between RT-D with DDA and CT. Based on the above results, CTL demonstrates a good agreement on the clustered porosity compared to the PAUT, the other NDT technique for access to depth information of inner imperfections. However, there are some differences in both measurements for other imperfections; lack of fusion and slag inclusion has been discussed since both techniques have advantages and capabilities in characterizing the imperfections. Furthermore, the physical appearance of imperfections could be influenced by the uncertainties of measurements for both techniques.

Author Contributions The manuscript was authored by SH and KA and reviewed by all authors. All shown figures are part of the laminography work performed at the Malaysian Nuclear Agency, funded by the

Data Availability Upon request.

Declarations

Competing interests Not Applicable.

Ethical Approval Yes.

Informed Consent Yes.

Consent for Publication Yes.

References

1. Brien, R.L.: Welding Handbook—Welding Science and Technology. American Welding Society, Miami (2001)
2. Ewert, U., Zscherpel, U., Bavendiek, K.: Replacement of film radiography by digital techniques and enhancement of image quality. NDT.net J. **6**, 4516 (2007)
3. Moreira, E.V., Barbosa Rabello, J.M., Pereira, M.D.S., Lopes, R.T., Zscherpel, U.: Digital radiography using digital detector arrays fulfills critical applications for offshore pipelines. EURASIP J. Adv. Signal Process. (2010). https://doi.org/10.1155/2010/894643
4. Bavendiek, K., Heike, U., Meade, W.D., Zscherpel, U., Ewert, U.: New digital radiography procedure exceeds film sensitivity considerably in aerospace applications. In: 9th European Conference on NDT (ECNDT 2006), pp. 1–16. NDT, Mayan (2006)
5. Boateng, F.T., Ewert, U., Kannengiesser, T., Zscherpel, U., Griesche, A., Kromm, A., Hohendorf, S., Redmer, B.: Real-time radiography for observation of crack growth during GTA welding. Weld. World IIW **60**(5), 931–937 (2016). https://doi.org/10.1007/s40194-016-0351-7
6. Van Tiggelen, R.: In search for the third dimension: from radiostereoscopy to three-dimensional imaging. JBR-BTR **85**, 266–270 (2002)
7. Kupsch, A., Trappe, V., Nielow, D., Schumacher, D., Lange, A., Hentschel, M.P., Redmer, B., Ewert, U., Bruno, G.: X-ray laminographic inspection of sandwich shell segments for wind turbine rotor blades. In: 12th European Conference on Non-destructive Testing, pp. 1–8. NDT, Mayan (2018)
8. Bullinger, O., Schnars, U., Schulting, D., Redmer, B., Tschaikner, M., Ewert, U.: Laminographic inspection of large carbon fibre composite aircraft-structures at airbus. In: 19th World Conference on Non-Destructive Testing, Proceedings, pp. 1–10. NDT, Mayan (2016)
9. Shen, Y., Morgeneyer, T.F., Garnier, J., Allais, L., Helfen, L., Crépin, J.: Three-dimensional quantitative in situ study of crack initiation and propagation in AA6061 aluminum alloy sheets via synchrotron laminography and finite-element simulations. Acta Mater. **61**(7), 2571–2582 (2013). https://doi.org/10.1016/j.actamat.2013.01.035
10. Moore, T.D., Vanderstraeten, D., Forssell, P.M.: Three-dimensional x-ray laminography as a tool for detection and characterization of BGA package defects. IEEE Trans. Components Packag. Technol. **25**(2), 224–229 (2002). https://doi.org/10.1109/TCAPT.2002.1010010

11. Wakimoto, K., Blunt, J., Carlos, C., Monteiro, P.J.M., Ostertag, C.P., Albert, R.: Digital laminography assessment of the damage in concrete exposed to freezing temperatures. Cem. Concr. Res. **38**, 1232–1245 (2008). https://doi.org/10.1016/j.cemconres.2008.05.003

12. Hamidi, S.H.A., Salleh, K.A.M., Hamzah, A.R., Wahab, M.N., Azaman, N., Ahmad, A.S.: Preliminary study of digital laminography parameters on carbon steel plate. IOP Conf. Ser. Mater. Sci. Eng. (2019). https://doi.org/10.1088/1757-899X/554/1/012007

13. Deyhle, H., Towsyfyan, H., Biguri, A., Mavrogordato, M., Boardman, R., Blumensath, T.: Spatial resolution of a laboratory based X-ray cone-beam laminography scanning system for various trajectories. NDT E Int. **111**(102222), 2020 (2020). https://doi.org/10.1016/j.ndteint.2020.102222

14. Fisher, S.L., Holmes, D.J., Jørgensen, J.S., Gajjar, P., Behnsen, J., Lionheart, W.R.B., Withers, P.J.: Laminography in the lab: Imaging planar objects using a conventional x-ray CT scanner. Meas. Sci. Technol. (2019). https://doi.org/10.1088/1361-6501/aafcae

15. O'Brien, N., Mavrogordato, M., Boardman, R., Sinclair, I., Hawker, S., Blumensath, T.: Comparing cone beam laminographic system trajectories for composite NDT. Case Stud. Nondestruct. Test. Eval. **6**, 56–61 (2016). https://doi.org/10.1016/j.csndt.2016.05.004

16. Kurfiss, M., Streckenbach, G.: Digital Laminography and Computed Tomography with 600 kV for Aerospace Applications. International symposium on NDT in Aerospace, Berlin (2012)

17. Yang, Y., Li, L., Chen, Z.: A review of geometric calibration for different 3-D X-ray imaging systems. Nucl. Sci. Tech. **27**(76), 1–11 (2016). https://doi.org/10.1007/s41365-016-0073-y

18. Thiessenhusen, K.U., Ewert, U., Redmer, B., Bavendiek, K.: Geometric corrections in coplanar translational laminography. In: International Symposium on Digital Industrial Radiology and Computed Tomography, pp. 1–8. NDT, Mayan (2011)

19. O'Brien, N.S., Boardman, R.P., Sinclair, I., Blumensath, T.: Recent advances in X-ray cone-beam computed laminography. J. Xray. Sci. Technol. **24**(5), 691–707 (2016). https://doi.org/10.3233/XST-160581

20. Zhou, J., Maisl, M., Reiter, H., Arnold, W.: Computed laminography for materials testing. Appl. Phys. Lett. **68**(24), 3500–3502 (1996). https://doi.org/10.1063/1.115771

21. Silva, W., Lopes, R., Zscherpel, U., Meinel, D., Ewert, U.: X-ray imaging techniques for inspection of composite pipelines. Micron **145**, 103033 (2021). https://doi.org/10.1016/j.micron.2021.103033

22. Ou, Y.X.D., Schumacher, D., Zscherpel, U.: Dual-energy materials characterization methods for laminography image enhancement based on photon counting detector. J. Instrum. **14**(P02018), 1–11 (2019). https://doi.org/10.1088/1748-0221/14/02/P02018

23. Ewert, U., Fuchs, T.: Progress in digital industrial radiology Part II: computed tomography (CT). Nondestruct. Test. Diagnostics **2**, 7–14 (2017). https://doi.org/10.26357/BNiD.2017.018

24. Varex (Perkin Elmer): Flat panel X-ray detectors. https://www.perkinelmer.com/PDFs/downloads/SPC-NDT-Detectors-012163A_01.pdf.

25. Ewert, U., Thiessenhusen, K., Deresch, A.: Reconstruction methods for coplanar translational laminography applications. In: Digital Industrial Radiology and Computed Tomography DIR 2015, pp. 1–21. NDT, Mayen (2015)

26. ISO 17636-2; Part 2: X- and gamma-ray techniques with digital detectors, (2013)

27. Hanif, S., Hamidi, A., Muad, A.M., Anuar, K., Salleh, M.: Development of a manipulator system for X-ray imaging laminography. J. Electr. Eng. **20**(2), 117–120 (2021)